

Long radial coherence of electron temperature fluctuations in non-local transport in HL-2A plasmas

Zhongbing Shi,* Kairui Fang, and Jie Wen, Zhanhui Wang, Xuantong Ding, Wei Chen, Zengchen Yang, Min Jiang Xiaoquan Ji, Ruihai Tong, Yonggao Li, Peiwang Shi, Wulyv Zhong, and Min Xu
Southwestern Institute of Physics, Post Office Box 432, Chengdu 610041, China

Jingchun Li, Zhaoyang Lu
*Department of Earth and Space Sciences, Southern University of Science and Technology,
 518055 Shenzhen, Guangdong, People's Republic of China*

Xiaolan Zou
CEA, IRFM, F-13108 Saint-Paul-lez-Durance, France
 (Dated: November 10, 2023)

The dynamics of long-wavelength ($k_\theta < 1.4 \text{ cm}^{-1}$), broadband (20-200 kHz) electron temperature fluctuations (\tilde{T}_e/T_e) of plasmas in gas-puff experiments were observed for the first time in HL-2A tokamak. In a relative low density ($n_e(0) \simeq 0.91 \sim 1.20 \times 10^{19}/\text{m}^3$) scenario, after gas-puffing the core temperature increases and the edge temperature drops. On the contrary, temperature fluctuation drops at the core and increases at the edge. Analyses show the non-local emergence is accompanied with a long radial coherent length of turbulent fluctuations. While in a higher density ($n_e(0) \simeq 1.83 \sim 2.02 \times 10^{19}/\text{m}^3$) scenario, the phenomena were not observed. Furthermore, compelling evidence indicates that $\mathbf{E} \times \mathbf{B}$ shear serves as a substantial contributor to this extensive radial interaction. This finding offers a direct explanatory link to the intriguing core-heating phenomenon witnessed within the realm of non-local transport.

PACS numbers: : 52.55.Tn, 52.25.Fi, 52.55.Fa, 52.70.Gw

I. INTRODUCTION

One of the perplexing phenomena observed and extensively studied worldwide is non-local transport, which has been investigated in various tokamaks (TFTR[1], TEXT[2]/J-TEXT[3], RTP[4, 5], HL-2A[6], Alcator C-mod[7], KSTAR[8], EAST[9], Tore Supra[10], JET[11], AUG[12], DIII-D[13]) and stellarators (W7-AS[14], LHD[15]). These experiments have consistently revealed a peculiar long-range transient temperature response triggered by pulsed interventions. These observations suggest that disturbances at the plasma's edge can perturb the deeper plasma equilibrium, challenging the conventional understanding of transport governed by local parameters and the gradient-flux relation[16, 17].

In recent years, turbulence theories focusing on multiple-scaled nonlinear and statistical dynamics have gained traction in addressing this enigma. These include turbulence spreading models[18–20, 22, 25] and the concept of self-organized criticality (SOC)[23–26]. Moreover, several studies propose that the transition between trapped electron modes (TEMs) and ion temperature gradient modes (ITGs) may play a role in the critical nature of non-local effects[27]. Evidence has emerged indicating the coexistence of rotation reversal, shear, and heat pinch phenomena[7, 8, 16, 28]. Notably, in the past year, a new form of non-locality in the ion temperature

channel was discovered in J-TEXT[29].

Despite more than two decades since its discovery, the mechanisms and theoretical models behind non-locality remain enduring enigmas in the field. In recent years, a particular perspective has emerged, challenging the traditional understanding of non-local transport. This perspective, supported by simulations, posits that the injection of a cold pulse may not actually induce genuine non-local transport[30, 31]. Instead, it suggests that non-locality can be explained as an outcome of the transient changes in local density gradients, with distinct mechanisms governing such behavior in plasmas dominated by TEMs versus ITGs[32–34].

Undoubtedly, local drift-wave turbulent transport mechanisms stand as widely accepted explanations for anomalous transport phenomena in tokamaks. Gyrokinetic and gyrofluid theories have been extensively validated and serve as robust frameworks for understanding these processes[34]. However, intriguingly, observations from experiments like EAST have revealed instances where density fluctuations transiently increase in the core before any local alterations in density and temperature occur[9]. Such findings hint at the possibility of a turbulence spreading model[22] at play. The question that looms large is how these turbulent fluctuations can evolve more rapidly than local profiles or gradients, a puzzle that demands further elucidation.

Hence, non-locality, to a certain extent, remains an enigma within the domain of heat transport. This perplexity arises from the challenges in deciphering thermal fluctuations within the turbulence. These fluctuations

*Electronic address: shizb@swip.ac.cn

are characterized by their low amplitude within the core region, their propensity for long-distance effects, and the formidable obstacles posed by localized measurements. Notably, the turbulence and its electron thermal fluctuation (referred to as \tilde{T}_e/T_e) present formidable detection and measurement challenges. This is exacerbated by the fact that the inherent thermal noise level is quite substantial, exceeding 4% of the temperature level, in stark contrast to the 1% threshold for \tilde{T}_e/T_e .

Thankfully, a ray of hope has emerged with the successful adaptation of correlation techniques initially developed for astronomical detection instruments into the realm of plasma diagnostics. A notable development on this front occurred last year with the deployment of a correlation electron cyclotron emission system (CECE) in the HL-2A tokamak. This advancement has played a pivotal role in shedding light on the profound physics underlying the non-local phenomenon. In this letter, we present a detailed analysis of electron temperature fluctuations, unveiling several groundbreaking findings for the first time.

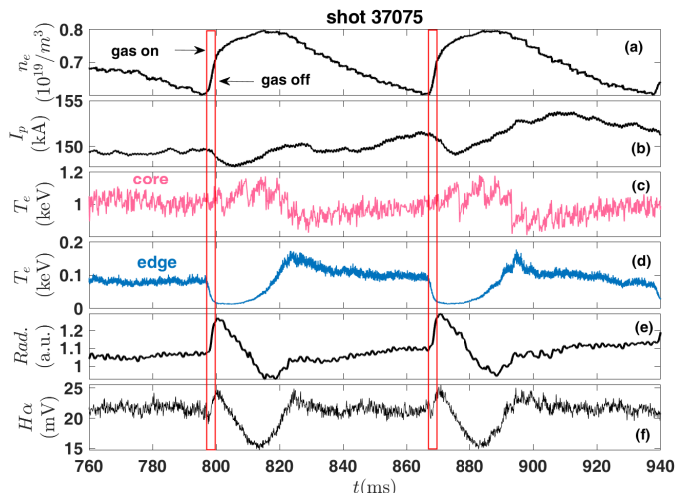


FIG. 1: Raw data in a non-local experiment (shot 37075). Time evolutions of (a) electron density from far infrared interferometer (FIR). (b) Plasma current. Electron temperature from ECE at (c) normalized radii $\rho \sim 0.10$ and (d) $\rho \sim 0.80$. (e) Power of plasma radiation from bolometer and (f) Raw signal of H_α radiation diagnostic. The perpendicular red lines represent the injection on and off, the same below.

II. EXPERIMENTAL SETUP

This study is based on data obtained from the HL-2A tokamak, a medium-sized device with a major radius (R) of 1.65 meters and a minor radius (a) of 0.4 meters [36]. The tokamak is equipped with a toroidal magnetic field ranging from 1.2 to 2.7 Tesla and is capable of generating plasma currents of up to 480 kiloamperes. The versatility of HL-2A allows for the investigation of

non-local transport effects through various experimental techniques, including modulated electron cyclotron heating (ECH), supersonic molecular beam injection (SMBI), pellet injection, gas puffing, fast current ramps, and laser blow-off [37]. In this particular study, we focus on non-local phenomena induced by gas puffing (GPs) in ohmic-heating plasmas characterized by relatively low electron densities (approximately $0.91 - 1.20 \times 10^{19}/m^3$). Key diagnostic tools employed include a multi-channel Electron Cyclotron Emission (ECE) system, which shares a common sightline and horn antenna with the CECE system, and a Doppler BackScattering (DBS) reflectometer located at a toroidal angle of 22.5 degrees relative to the ECE window [38]. The DBS instrument provides valuable information about plasma rotation, density fluctuations, and radial electric fields.

III. EXPERIMENTAL RESULTS

A. General non-local phenomenon in GP experiment

Figure 1 illustrates various parameters observed during a typical discharge involving multiple Gas Puffs (GPs). In this experimental shot, the plasma is subjected to ohmic heating, featuring a toroidal magnetic field configuration of 1.34 T and a plasma current of approximately 150-153 kA. Each gas puff lasts for about 1-2 ms, which is similar in duration to Supersonic Molecular Beam Injections (SMBIs) but with lower pulse intensity. The on/off timing of the GPs is indicated by the front and rear red lines perpendicular to the time axis. It's crucial to note that the time intervals between these pulses are sufficiently long to ensure the independence of each non-local transport effect.

Additionally, the plasma density (Figure 1(a)) is measured using a far-infrared interferometer (FIR) [39]. It's evident that the line-averaged density increases immediately after the GPs and then gradually decreases. Simultaneously, the inner core electron temperature exhibits a bulge, followed by a recovery over a duration of approximately 30 ms, while the edge amplitudes undergo opposite changes. The evolution of plasma current, radiation power, and H_α signals are also displayed.

The foundational investigation commences with equilibrium parameters because local collisionality and gradients in the background are likely to influence the turbulent state, subsequently affecting the measurements. Figure 2(a) presents the time traces of electron temperature (T_e) signals at different radial positions. It's important to emphasize that the puff time is normalized to zero with the onset of gas injection, facilitating a clearer time series for signal comparison. The heat diffusivity induced by sawtooth oscillations ranges from 4-6 m^2/s at $\rho \simeq 0.5$, with no discernible variation before and after the occurrence of non-local phenomena. The puffs in the experiment are deployed beyond $\rho > 0.7$, resulting

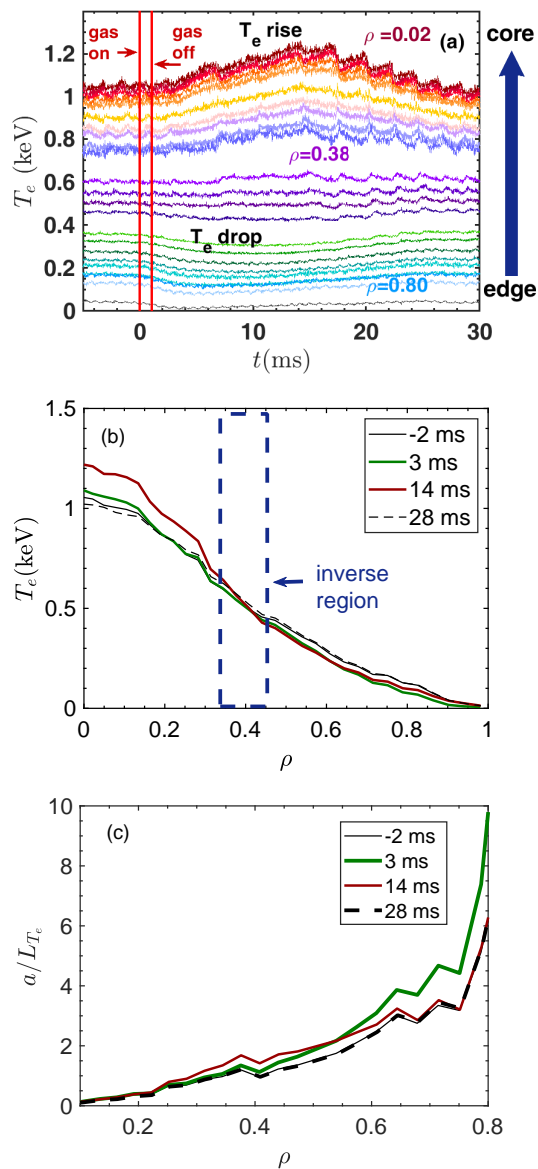


FIG. 2: (a) Electron temperature from plasma edge to the core. The gas is fed at 0 ms. Profiles of (b) electron temperature and (c) normalized T_e gradient scale length at 2 ms before, 3 ms after, 14 ms after ($T_e(0)$ peaking) and 28 ms after (recovery).

in immediate changes in edge profiles. Figure 2(b) and 2(c) display profiles of electron temperature (T_e) and the normalized gradient scale length a/L_{T_e} before, during, and after the non-local effect. Negative time values represent the period before puffing when parameters serve as references. In Figure 2(b), we observe a rapid change in T_e occurring first outside the inverse radius, peaking with a delay of approximately 2-3 ms. Subsequently, the core region of T_e begins to rise, with a maximum increment of about 18% (approximately 200 eV) observed in the central core at around 14 ms. Regarding the normalized gradient scale length a/L_{T_e} presented in Figure

2(c), local a/L_{T_e} variations are consistent with local T_e over time. In contrast, a/L_{T_e} displays a global increase following the gas puff.

B. Non-locality in electron temperature fluctuations

Figure 3(a-c) illustrates the coherencies, while figure 3(d-f) displays normalized time-domain fluctuations ($\tilde{T}_e/T_e(t)$) integrated within the 20-200 kHz frequency range. Evidently, following the gas puff, there is a rapid and significant increase in the amplitude of relative electron temperature fluctuations, primarily observed at the peripheral radius around $\rho \simeq 0.80$. This observation is substantiated by both the coherency graphs and the $\tilde{T}_e/T_e(t)$ plots. Moving closer to the location of the T_e inverse radius, there is a diminished distinction between the two phases. Conversely, at the edge, during the non-local phase, $\tilde{T}_e/T_e(t)$ decreases in the central core. Reflecting on the previous T_e response, the behavior of these fluctuations aligns with the T_e increment/decrement, as a greater/lower fluctuation amplitude corresponds to stronger/weaker turbulence and more/less heat transport (heat loss), assuming other conditions remain constant. Notably, the CECE-measured fluctuations have been previously linked to ∇T_e driving in ohmic heated L-mode plasma, a concept widely accepted in drift-wave turbulence theories[35].

This study also undertakes a similar comparison between a/L_{T_e} and \tilde{T}_e/T_e . One of the outcomes, at $\rho \sim 0.09$, is presented in figure 4. Interestingly, unlike the typical gradient-flux relation, fluctuations in this scenario exhibit a decrease in amplitude alongside the local gradient of a/L_{T_e} , with the latter remaining relatively unchanged (slightly increasing). This finding suggests that fluctuations in the region of $\rho < 0.30$ are not primarily determined by local a/L_{T_e} ; in other words, the steady-state gradient driving is not applicable in this context. For electrostatic turbulence, another possibility considered is the role of ∇n_e driving. However, validating this mechanism presents challenges, primarily due to limited means of locally measuring core density. While the interferometer with tomographic inversion can reconstruct the density profile, it may introduce distortion in the signal evolution in the core due to edge data interference. Conversely, in the peripheral region, the local gradient and \tilde{T}_e/T_e can be associated since the relationship between figure 2(c) and 3(d) demonstrates a positive correlation. Notably, no significant changes were observed in coherency and fluctuation evolution around the T_e inverse radius.

Using multiple radial positions, the profile of \tilde{T}_e/T_e can be constructed, as depicted in Figure 5(a). In light of the preceding analyses, it becomes apparent that the \tilde{T}_e/T_e profile also exhibits an inverse radius when computed with and without the non-local phases. Furthermore, additional radial cross coherency analyses were conducted,

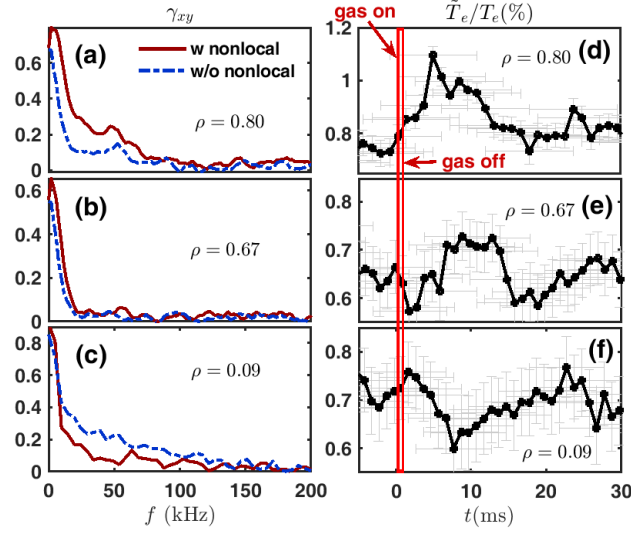


FIG. 3: (a-c) Cross coherencies calculated during the nonlocal phases (w nonlocal) and the steady state phases (w/o nonlocal) at different radii and (d-f) Time sequences with \tilde{T}_e/T_e (20-200kHz).

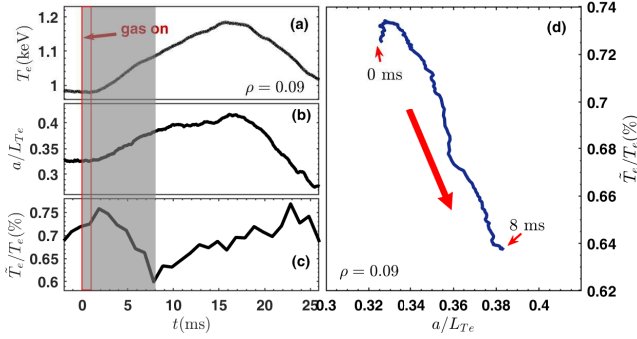


FIG. 4: Evolution of local ($\rho = 0.09$) (a) electron temperature (b) normalized gradient length of a/L_{Te} and (c) relative fluctuations of \tilde{T}_e/T_e . (d) Relation between a/L_{Te} and \tilde{T}_e/T_e . Several core data points imply fluctuations are not mainly driven by the temperature gradients.

focusing on specific channels in relation to others, as illustrated in Figure 5(b). Specifically, the channel at $\rho = 0.80$ was selected as a reference point. The radial coherence length (L_c) was theoretically defined as the radial span over which the integrated coherencies or fluctuations diminish to $1/e$ of their amplitude.

Following the gas puffing, the radial coherence length experiences a significant increase during the non-local phases, as evident in Figure 5(b). During the steady phase, the observed radial coherence extends approximately 2.5 cm, but this length escalates to about 8.8 cm during the non-local phase. Given the selected channel at $\rho = 0.80$, this result suggests that the long radial influence penetrates to approximately $\rho \sim 0.55$, precisely within the vicinity of the T_e inverse region. Furthermore, the observed radial coherence effect persists, man-

ifesting as a non-Gaussian tail extending approximately 22 cm, signifying profound and deeper transient interactions. This phenomenon also implies that long radial coherent turbulences are established immediately after the gas puffs [Figure 5(c)].

In conjunction with the response time illustrated in Figure 3(d-f), the alterations in coherent length are consistent with fluctuations in amplitude. These observations of long-distance coherence or correlation likely constitute a mechanism for radial transient transport. Furthermore, L_c is determined by integrating fluctuations within the 20-200 kHz frequency range to mitigate the influence of low-frequency MHD interference. This represents a significant advancement compared to previously reported macroscopic structures in some instances.

It is noteworthy that the measurement principle of ECE involves utilizing two adjacent channels with very close frequencies for correlation analysis to eliminate the influence of noise. As illustrated in Figure 1 (see ref. [35]), the bandwidth of the adjacent channels is 150 MHz, corresponding to a spatial width of approximately 1 cm. Due to radiation broadening, there is some overlap between measurements from these two channels. When the two channels are measured independently, turbulence exhibits spatial correlation, while noise lacks correlation, thus achieving the objective of noise reduction. Moreover, in the high-frequency range, the correlation is relatively weak. Although the correlation is weak around 100-200 kHz at $\rho \sim 0.8$, it remains evident when comparing cases with and without non-local phenomena. Additionally, to eliminate the influence near zero frequency, signals in the 0-20 kHz range were not considered. Therefore, a range of 20-200 kHz was employed in this study. In fact, the choice of frequency range has no impact on the results presented in Figure 3.

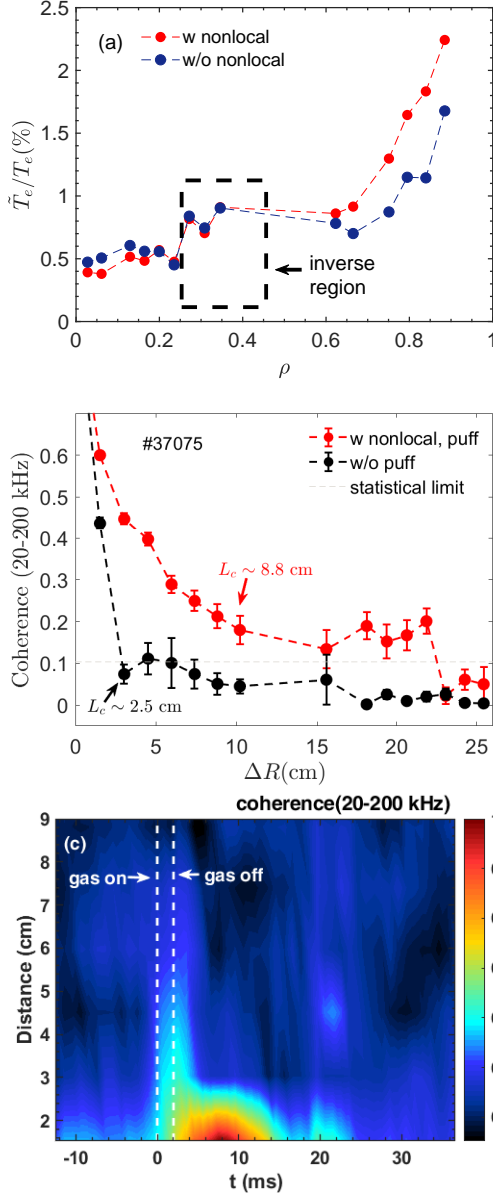


FIG. 5: (a) Relative electron temperature fluctuation profile of \tilde{T}_e/T_e (%) (20-200kHz). (b) Radial coherent length with reference position at $\rho = 0.80$ and (c) spatiotemporal structure of coherent length in the low density scenario.

C. A comparison between low- and high-density scenario

Before delving into comparative scenarios, it is imperative to juxtapose the performance of \tilde{T}_e/T_e with density fluctuations derived from DBS data. Within the DBS system, the meso-scale portion (20-100 kHz) of the spectrum demonstrates a degree of consistency with \tilde{T}_e/T_e . However, it is worth noting that due to the distinct wavenumbers detected (with k_\perp falling in the range of $4\text{--}10\text{ cm}^{-1}$ by the DBS and k_θ remaining below 1.4 cm^{-1})

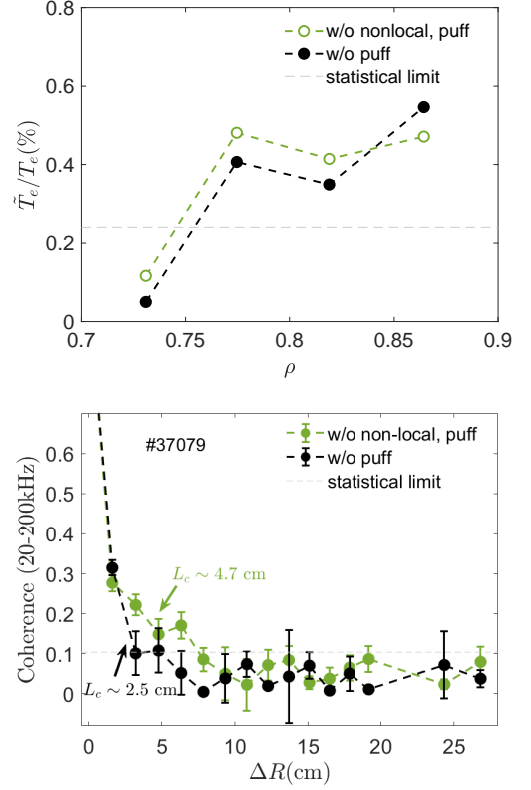


FIG. 6: (a) Profile of \tilde{T}_e/T_e . (b) Radial coherent length with reference of $\rho = 0.86$ in the high density ($n_e(0) \simeq 1.83 \sim 2.02 \times 10^{19}/m^3$) scenario. There is no obvious difference between phase before and after the gas puff.

via the CECE system, higher-frequency (≤ 100 kHz) density fluctuations exhibit dissimilar behavior. This observation aligns with previous reports from HL-2A[16, 43].

It's important to highlight that cross-correlation analysis between \tilde{n}_e and \tilde{T}_e was not conducted in this study. Nonetheless, an alternative and valuable physical parameter can be derived - the perpendicular velocity, as it is closely related to the Doppler shift ($v_\perp(\rho, t) = 2\pi f_d/k_\perp$). In a broad sense, v_\perp can be considered as the sum of $v_{E \times B}$ and v_ϕ when v_ϕ is negligibly small compared to $v_{E \times B}$ at the plasma edge. Subsequently, $v_{E \times B}$ is associated with the $E \times B$ shearing rate:

$$\gamma_{E \times B} = (r/q)d(E_r/B_p R)/dr \sim \frac{\partial v_{E \times B}}{\partial r} \quad (1)$$

where q represents the safety factor, and B_p signifies the poloidal magnetic field. As is well-established, turbulence suppression takes place when the $E \times B$ shearing rate surpasses the linear growth rate of the underlying instability, and conversely[44]. Given that the measured velocities are primarily influenced by $E \times B$ shear, all other factors being constant, one can estimate the evolution of $\gamma_{E \times B}$.

A high-density scenario ($n_e(0) \simeq 1.83 \sim 2.02 \times$

$10^{19}/m^3, I_p \simeq 160kA$) was investigated while maintaining consistent puff intensity. Using data from the DBS reflectometer, electron temperature fluctuations in the high-density scenario were investigated and are presented in figure 6. In figure 6(a), the profile for this scenario is displayed, while figure 6(b) shows the radial coherent length. The \tilde{T}_e/T_e was also integrated with 20-200 kHz coherencies to obtain the normalized coherence (20-200 kHz). The legend "w/o nonlocal, puff" indicates the period of T_e drop after puffing, while "w/o puff" corresponds to the steady-state phase. In contrast to figure 5, the \tilde{T}_e/T_e and coherent length exhibit smaller increases during the non-steady state. Importantly, the coherence entirely dissipates at $\rho \sim 0.65$. This suggests that edge puffing has minimal influence on the core in the context of relatively higher-density plasma. For the central \tilde{T}_e/T_e , the fluctuation amplitudes remain below the noise level and cannot be reliably extracted.

Furthermore, Figure 7 displays the $E \times B$ shearing rates ($\gamma_{E \times B}$) for this particular scenario (shot 37079) alongside data from shot 37075. The polarity of v_\perp signifies ion or electron diamagnetic drift direction, respectively. It's evident that the $E \times B$ flow experiences transient variations after the puffs in both scenarios. In shot 37079, v_\perp at all detected radii decelerates, causing shear rates to immediately decline with an inward propagation damping effect. Conversely, in the low-density scenario, the reduction in $\gamma_{E \times B}$ persists in the peripheral region. However, the propagation dynamics shift within $\rho = 0.52$. Instead, v_\perp and $\gamma_{E \times B}$ show rapid increases after the puffs, a phenomenon distinct from the high-density scenario. Notably, the point at which shear rates begin to change aligns closely with the T_e inverse radius. In both scenarios, the trends in shear rates in the central region are consistent with their impact on $\tilde{T}_e/T_e(t)$.

These findings align closely with the critical gradient model described in previous works[21]. To elucidate further, considering the radial dimension, it can be expressed as follows:

$$\frac{\partial I}{\partial t} - \frac{\partial}{\partial \rho}(\hat{\chi}_{turb} \frac{\partial I}{\partial \rho}) = \hat{\gamma}I - \hat{\beta}I^2, \quad (2)$$

$$\frac{\partial \langle \hat{T} \rangle}{\partial t} - \frac{\partial}{\partial \rho}[(\hat{\chi}_{turb} + \hat{\chi}_{neo}) \frac{\partial \langle \hat{T} \rangle}{\partial \rho}] = \hat{S}, \quad (3)$$

where the normalized quantities are denoted with a superscript $\hat{\cdot}$ and the normalized process was described in [21]. Here, I is the turbulence intensity, β is local non-linear damping rate, $\hat{\chi}_{turb} = \hat{\chi}_0 I / (1 + \hat{A}^2 / \hat{\kappa}_c^2)$ is the normalized turbulent thermal diffusivity, $\hat{\chi}_{neo}$ is the normalized neoclassical thermal diffusivity, \hat{S} is the normalized heating source and $\hat{\gamma} = \hat{\gamma}_0 \hat{R}(\hat{A} - \hat{A}_{crit})\Theta(\hat{A} - \hat{A}_{crit}) / (1 + \hat{A}^2 / \hat{\kappa}_c^2)$ is the local growth rate of turbulent intensity with a Heviside function Θ . $\hat{A} = |\partial \langle \hat{T} \rangle / \partial \rho|$ is the magnitude of the local mean temperature (ion or electron) gradient. The electric field shear is related to local parameter with $\hat{\kappa}_c^2$. Notably, turbulence spreading exhibits a velocity of

$\hat{v}f \sim \sqrt{\hat{\gamma} \hat{\chi}_{turb}}$, which is comparable to the Fisher front speed[45, 46]. It has been demonstrated in simulations that with strong shearing (smaller $\hat{\kappa}_c$) and weak shearing, a bifurcation of T_e can be achieved[21].

IV. CONCLUSION AND DISCUSSION

This study sheds light on the intricate dynamics of turbulence, which play a pivotal role in non-local transport effects in tokamak plasmas [47–49]. Leveraging advanced core detection and measurement techniques, our analyses unveil the behavior of non-local transport in low-density plasmas, intricately linked with the broadband (20-200 kHz) electron temperature fluctuations. Both our findings in the frequency domain through cross-coherence analysis and the time-domain $\tilde{T}_e/T_e(t)$ demonstrate that transient changes are intimately associated with turbulent dynamics. During non-locality phases, the \tilde{T}_e/T_e temporal profiles exhibit marked differences between the central and edge regions. Consequently, we challenge the conventional understanding of local a/L_{T_e} driving mechanisms. Furthermore, our observations reveal the rapid formation of long radial coherent fluctuations, with coherence lengths comparable to the plasma size (approximately $0.5a$). This phenomenon arises immediately after pulse injection, effectively breaking down local transport relations. In essence, transient transport can be initiated by distant effects.

Simultaneously investigating plasma rotation, we identify a partial alignment between $E \times B$ flow shear and the transient fluctuation changes, without accounting for instability growth rates. However, in a comparative high-density scenario, our observations manifest stark differences, with no clear indications of core-edge transient interactions. When the non-local conditions are met, particularly in scenarios characterized by lower density and larger plasma current, we observe a simultaneous decrease in flow shearing rates and rapid turbulence growth in the same region. This observation suggests that flow shearing rates could significantly contribute to the formation of long radial coherent structures due to their interplay with turbulence. Our direct observations show an increase in core shear rates within 1-2 ms, which corresponds to transient changes in \tilde{T}_e/T_e . Notably, this propagation speed of amplitude change is on the order of 10^2 m/s, far exceeding the device's global confinement time of 30 ms. Considering that the inward coherent length extends to approximately 8.8 cm with the reference at $\rho = 0.80$, it encompasses a significant portion of the plasma's minor radius.

In addition, these observations are contingent on diagnostic compatibility, which can be further optimized. For instance, the measured \tilde{T}_e/T_e profile exhibits a steep decay, reaching noise levels at relatively peripheral radii. This limitation could be mitigated by employing a smaller beam size or extending the Rayleigh length of the diagnostic sight. Additionally, the v_\perp of the flow will

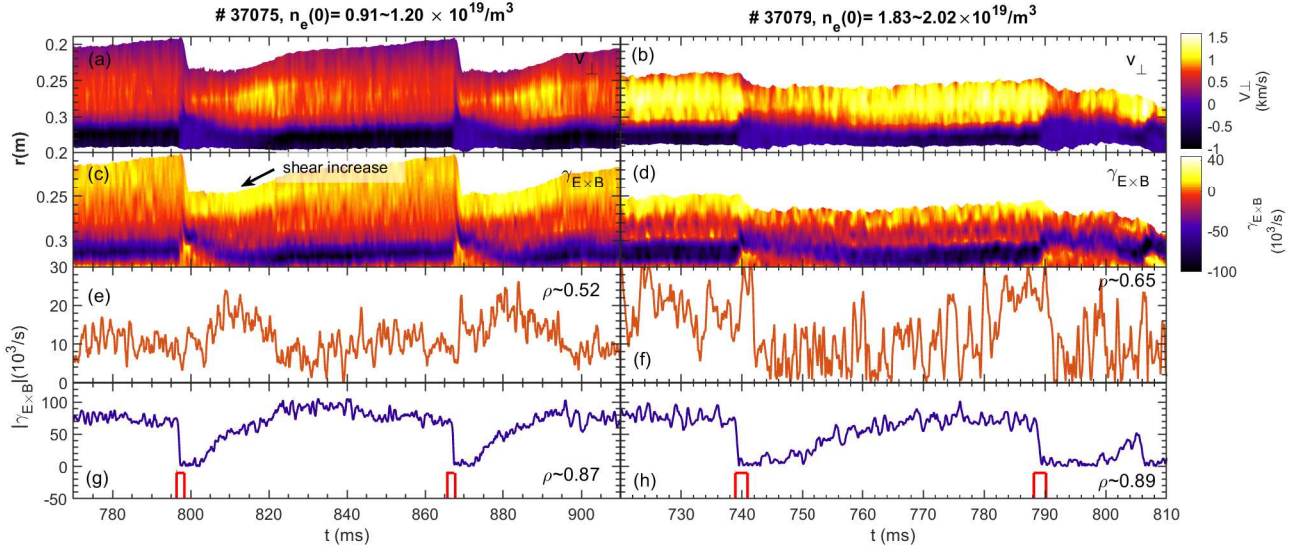


FIG. 7: Spatiotemporal plots of (a-b) Perpendicular velocities v_{\perp} , (c-d) $E \times B$ shear rates $\gamma_{E \times B}$ and (e-h) absolute values of $\gamma_{E \times B}$ with core T_e increase (nonlocal phenomenon) in the low density ($n_e(0) \simeq 0.91 \sim 1.20 \times 10^{19}/m^3$) scenario and without core T_e increase in the high density ($n_e(0) \simeq 1.83 \sim 2.02 \times 10^{19}/m^3$) scenario. The plus or minus value of v_{\perp} represents the ion or electron diamagnetic drift direction, respectively. The shearing rates increase abruptly inside inverse region in the non-local scenario.

be detected in the central core using a higher radio frequency of the reflectometer. The observed fluctuation bifurcation hints at the potential formation of a barrier-like structure, akin to a transient internal transport barrier (ITB) [50], in the inverse region. Evidence of interactions between shear profiles and structures can also be gleaned from comparative experiments, where the location of the barrier (sudden change) varies. Importantly, these results are corroborated by their disappearance or significant weakening in scenarios without non-locality.

In general, local plasma parameters play a pivotal role in driving instabilities, such as pressure gradients, ion and electron temperature gradients. Even in cases of non-diffusive momentum transport, which falls under the umbrella of locality since these non-diffusive terms are determined by local parameters, non-local transport exhibits a clear departure from local closure. Non-local transport encompasses the influence of parameters located far from where the transport occurs, challenging the notion that electrostatic turbulence alone dictates heat flux. Instead, it is primarily determined by the coupling between turbulence and electric fluctuations. Nonetheless, the

presence of shear and long radial coherence in electron temperature fluctuations provides valuable insights. This study does not delve into other processes, such as nonlinear multi-scale turbulent interactions, turbulence spreading, and density-temperature bicoherence. However, it's worth noting that in the theory of self-organized criticality, enhanced avalanches can occur when a long radial correlation is present [51]. This could potentially serve as a mechanism for transient flow variations. To conduct a comprehensive investigation, future experiments will explore electric field, density, and temperature channels.

Acknowledgement The authors thank to Prof. Inagaki for useful analytic discussions in APTWG meeting. This work is partly supported by National Key R&D Program of China (Grant Nos. 2017YFE0301203, 2017YFE0301106), Sichuan Science and Technology Program (Grant No. 2018RZ0123, 2021YFSY0044), National Natural Science Foundation of China (Grant Nos. 12175055), and Shenzhen Municipal Collaborative Innovation Technology Program-International Science and Technology Cooperation Project (GJHZ20220913142609017).

- [1] Kissick M W, Fredrickson E D, Callen J D, Bush C E, Chang Z, Efthimion P C, Hulse R A, Mansfield D K, Park H K, Schivell J F, Scott S D 1994 *Nuclear fusion* **34** 349
- [2] Gentle K W, Rowan W L, Bravenec R V, Cima G, Crowley T P, Gasquet H, Hallock G A, Heard J, Ouroua A, Phillips P E, Ross D W 1995 *Physical review letters* **74** 3620
- [3] Shi Y, Chen Z, Yang Z, Shi P, Zhao K, Diamond PH, Kwon J, Yan W, Zhou H, Pan X, Cheng Z. Observation of multi-

channel non-local transport in J-TEXT plasmas 2018 *Nuclear Fusion* **58** 044002

- [4] Galli P, Gorini G, Mantica P, Hogeweij GM, De Kloe J, Cardozo NL, RTP team 1999 *Nuclear Fusion* **39** 1355
- [5] Mantica P, Galli P, Gorini G, Hogeweij GM, De Kloe J, Cardozo NL, RTP Team 1999 *Physical review letters* **82** 5048
- [6] Hong-Juan S, Xuan-Tong D, Liang-Hua Y, Bei-Bin F, Wei L, Yu-Dong P, Ze-Tian L, Xu-Ru D, Qing-Wei Y, Yong L 2007

Chinese Physics Letters **24** 2621

- [7] Rice J E, Gao C, Reinke M L, Diamond P H, Howard N T, Sun H J, Cziegler I, Hubbard A E, Podpaly Y A, Rowan W L, Terry J L 2013 *Nuclear Fusion* **53** 033004
- [8] Shi Y J, Kwon J M, Diamond P H, Ko W H, Choi M J, Ko S H, Hahn S H, Na D H, Leem J E, Lee J A, Yang S M 2017 *Nuclear Fusion* **57** 066040
- [9] Liu Y, Shi Y, Zhang T, Zhou C, Zou X, Zhao H, Liu A, Zhou T, Liu X, Zhang S, Cao B 2019 *Nuclear Fusion* **59** 044005
- [10] Zou X L, Geraud A, Gomez P, Mattioli M, Segui J L, Claret F, De Michelis C, Devynck P, de Wit TD, Erba M, Fenzi C 2000 *Plasma physics and controlled fusion* **42** 1067
- [11] Gorini G, Joffrin E, Mantica P, Sarazin Y, Challis C D, Coffey I, Kinsey J E, Litaudon X, Sozzi C, Walden A, Zastrow K D 2001 *28th EPS Conference on Contr. Fusion and Plasma Phys. Funchal* **25A** 497
- [12] Ryter F, Neu R, Dux R, Fahrbach H U, Leuterer F, Pereverzev G, Schweinzer J, Stober J, Suttrop W, De Luca F, Jacchia A 2000 *Nuclear fusion* **40** 1917
- [13] Rodriguez-Fernandez P, White A E, Howard N T, Grierson B A, Zeng L, Yuan X, Staebler G M, Austin M E, Odstrcil T, Rhodes T L, Sciortino F 2019 *Physics of Plasmas* **26** 062503
- [14] Stroth U, Giannone L, Hartfuss HJ, ECH group, W7-AS team 1996 *Plasma Physics and Controlled Fusion* **38** 611
- [15] Inagaki S, Tamura N, Tokuzawa T, Ida K, Itoh K, Neudatchin SV, Tanaka K, Nagayama Y, Kawahata K, Yakovlev M, Sudo S 2006 *Plasma physics and controlled fusion* **48** A251
- [16] Ida K, Shi Z, Sun H J, Inagaki S, Kamiya K, Rice J E, Tamura N, Diamond P H, Dif-Pradalier G, Zou X L, Itoh K 2015 *Nuclear Fusion* **55** 013022
- [17] Inagaki S, Tokuzawa T, Tamura N, Itoh S I, Kobayashi T, Ida K, Shimozuma T, Kubo S, Tanaka K, Ido T, Shimizu A 2013 *Nuclear Fusion* **53** 113006
- [18] Hahm T S, Diamond P H, Lin Z, Itoh K, Itoh S I 2004 *Plasma physics and controlled fusion* **46** A323
- [19] Gurcan O D, Diamond P H, Hahm T S, Lin Z 2005 *Physics of plasmas* **12** 032303
- [20] Lin Z, Hahm T S 2004 *Physics of Plasmas* **11** 1099
- [21] Wang Z H, Diamond P H, Gurcan O D, Garbet X, Wang X G 2011 *Nuclear Fusion* **51** 073009
- [22] Hariri F, Naulin V, Juul Rasmussen J, Xu G S, Yan N 2016 *Physics of Plasmas* **23** 052512
- [23] Diamond P H, Hahm T S 1995 *Physics of Plasmas* **2** 3640
- [24] Kubota T, Iwasaki T, Itoh S I, Yagi M, Fukuyama A, Stroth U 1997 *24th EPS Conference on Controlled Fusion and Plasma Physics* 1769
- [25] Wang Z H, Diamond P H, Gurcan O D, Garbet X, Wang X G 2011 *Physics of Plasmas* **18** 032306
- [26] Chen W, Xu Y, Ding X T, Shi Z B, Jiang M, Zhong W L, Ji X Q 2016 *Nuclear Fusion* **56** 044001
- [27] Gao C, Rice J E, Sun HJ, Reinke M L, Howard N T, Mikkelsen D, Hubbard A E, Chilenski M A, Walk J R, Hughes J W, Ennever PC 2014 *Nuclear Fusion* **54** 083025
- [28] Mantica P, Gorini G, Hogeweij G M, Carodozo N L, Schilham A M 2000 *Physical review letters* **85** 4534
- [29] Shi Y, Yang Z, Chen Z, Cheng Z, Zhang X, Yan W, Wen J, Cai Q, Zhao K, Hong S, Kwon J 2020 *Nuclear Fusion* **60** 064002
- [30] Rodriguez-Fernandez P, White A E, Howard N T, Grierson B A, Staebler G M, Rice J E, Yuan X, Cao N M, Creely A J, Greenwald M J, Hubbard A E 2018 *Physical review letters* **120** 075001
- [31] Angioni C, Fable E, Ryter F, Rodriguez-Fernandez P, Putterich T, ASDEX Upgrade Team 2019 *Nuclear Fusion* **59** 106007
- [32] Li J C, Liu S F, Kong W, Guo S C, Dong JQ 2019 *Europhysics Letters* **127** 45002
- [33] Li J, Lin Z, Dong J, Xie H, Liu S 2021 *Plasma Physics and Controlled Fusion* **63** 125005
- [34] Li J, Xu J Q, Qu Y R, Lin Z, Dong JQ, Peng X D, Li J Q 2023 *Nuclear Fusion* **63** 096005
- [35] Fang K R, Shi Z B, Yang Z C, Jiang M, Zhong W L, Wen J, Shi P W, Li Y G, Liu Z T, Liu Y, Ding X T 2019 *Review of Scientific Instruments* **90** 063503
- [36] Liu D, Zhou C, Cao Z, Yan J, Liu Y, The HL-2A Team. 2003 *Fusion Engineering and Design* **66** 147
- [37] Sun H J, Ding X T, Yao L H, Rao J, Liu ZT, Liu Y, Huang Y, Dong C F, Li W, Duan X R, Yan QW 2008 *Journal of Physics: Conference Series* **123** 012016
- [38] Shi Z, Zhong W, Jiang M 2018 *Plasma Science and Technology* **20** 094007
- [39] Li Y G, Zhou Y, Li Y, Deng Z C, Wang H X, Yi J 2017 *Review of Scientific Instruments* **88** 083508
- [40] Greenwald M, Terry J L, Wolfe S M, Ejima S, Bell M G, Kaye S M, Neilson G H 1988 *Nuclear Fusion* **28** 2199
- [41] Creely A J, Freethy S J, Burke W M, Conway G D, Leccarcorvi R, Parkin W C, Terry D R, White A E 2018 *Review of Scientific Instruments* **89** 053503
- [42] Inagaki S, Tokuzawa T, Itoh K, Ida K, Itoh SI, Tamura N, Sakakibara S, Kasuya N, Fujisawa A, Kubo S, Shimozuma T 2011 *Physical review letters* **107** 115001
- [43] Shi Z 2018 *APS Division of Plasma Physics Meeting Abstracts*
- [44] Schirmer J, Conway G D, Zohm H, Suttrop W, ASDEX Upgrade Team 2006 *Nuclear fusion* **46** S780
- [45] Fisher R A 1937 *Annals of Eugenics* **7** 355
- [46] Alonso J A, Sanchez E, Calvo I, Velasco J L, McCarthy K J, Chmyga A, Eliseev L G, Estrada T, Kleiber R, Krupnik L I, Melnikov A V 2017 *Physical Review Letters* **118** 185002
- [47] Li J C, Dong J Q, Ji X Q, Hu Y J *Chinese Physics B* 2021 **30** 075203
- [48] Li J C, Gong X Y, Dong J Q, Wang J, Yin L *Chinese Physics B* 2016 **25** 045201
- [49] Jiao Y M, Yao L H, Feng B B, Chen Ch Y, Zhou Y, Shi Z B, Dong J Q, Duan X R *ACTA PHYSICA SINICA* 2010, **59** 7191
- [50] Xu J Q, Peng X D, Hao G Z, Chen W, Li J Q, Qu H P, Li J C, Ren G Z, He X X, Li Y G *Physics of Plasmas* 2022 **29** 012508
- [51] Pan O, Xu Y, Hidalgo C, Zhong W L, Shi ZB, Ji X Q, Jiang M, Feng B B, Zhou Y, Cheng J, Liu Y 2015 *Nuclear Fusion* **55** 113010